Research article **Open Access**

Yonatan Sivan* and Shi-Wei Chu

Nonlinear plasmonics at high temperatures

DOI 10.1515/nanoph-2016-0113
Received March 31, 2016; revised June 7, 2016; accepted July 10, 2016

Abstract: We solve the Maxwell and heat equations self-consistently for metal nanoparticles under intense continuous wave (CW) illumination. Unlike previous studies, we rely on *experimentally-measured* data for metal permittivity for increasing temperature and for the visible spectral range. We show that the thermal nonlinearity of the metal can lead to substantial deviations from the predictions of the linear model for the temperature and field distribution and, thus, can explain qualitatively the strong nonlinear scattering from such configurations observed experimentally. We also show that the incompleteness of existing data of the temperature dependence of the thermal properties of the system prevents reaching a quantitative agreement between the measured and calculated scattering data. This modeling approach is essential for the identification of the underlying physical mechanism responsible for the thermo-optical nonlinearity of the metal and should be adopted in all applications of high-temperature nonlinear plasmonics, especially for refractory metals, for both CW and pulsed illumination.

Keywords: thermoplasmonics; nonlinear optics; metal nanoparticles.

1 Introduction

Nanoplasmonic systems have been intensively studied in recent decades due to their unique potential for local field enhancement and subwavelength confinement and are considered as promising candidates for a wide variety of applications [1, 2]. However, the inherent absorption in the metal proves to be a substantial obstacle toward the realization of real-life applications.

Accordingly, in recent years, the applied plasmonic research focused on applications that *exploit* the absorption in the metal as a means to generate heat on the nanoscale [3, 4] – a research topic usually referred to as thermoplasmonics. This resulted in a wide range of emerging applications, at different ranges of temperatures, starting from photothermal (PT) imaging [5, 6], through cancer treatment [7], temperature measurement [8], plasmonic photovoltaics [9] and water boiling, sanitation, and superheating [10–13], up to thermophotovoltaics [14, 15], diffusive switching [16], radiative heat transfer [17], plasmon-mediated photocatalysis [18–20], plasmon-assisted chemical vapor deposition [21], and heat-assisted magnetic recording [22], which may involve temperatures even higher than 2000 K.

In the majority of works in thermoplasmonics, the optical and thermal properties are assumed to be fixed. However, as the heat is induced by laser illumination (unlike external heating assumed in thermal emission engineering and nanoscale radiative heat transfer [23, 24]), it is necessary to account for the coupling between the electromagnetic fields, the temperature, the optical properties, and the thermal properties (i.e. heat capacity, thermal conductivity, and Kapitza resistance) of the constituents to achieve a quantitative understanding of the field and temperature distribution. To the best of our knowledge, such a systematic, self-consistent study was not performed so far in the context of thermoplasmonics. Specifically, the temperature dependence of metal permittivity was accounted for in some studies either through a (cubic) thermal nonlinearity [25, 26] or, more generally, based on a combination of the two-temperature model [27] with a complex model of the permittivity. Such models have to correctly account for a rather large number of competing effects within the metal, including electron scattering, thermal expansion, band shifting, the effect of Fermi smearing on intraband transitions [25] and interband transitions [28–30], and more. To the best of our knowledge, such a comprehensive study was done only by Stoll et al. [31]. Moreover, during intense illumination, all the effects mentioned above are modified due to the deviation of the electron distribution function, scattering rates, etc., from their

***Corresponding author: Yonatan Sivan,** Unit of Electro-optics Engineering, Faculty of Engineering Sciences, Ben-Gurion University of the Negev, P.O. Box 653, Beersheba 8410501, Israel, e-mail: sivanyon@bgu.ac.il
Shi-Wei Chu: Department of Physics, National Taiwan University, No. 1, Sec. 4, Roosevelt Road, Taipei 10617, Taiwan

equilibrium values – effects that were studied only partially [25, 32–34]. Most importantly, the studies such as [25–34], and the many less complete ones, were all dedicated to the ultrafast regime, such that efforts were made to avoid the longer-term (i.e. few picoseconds and longer) thermal effects, for example, by looking at nanoparticles (NPs) not larger than a few nanometers in diameter, lowering the repetition rate, etc. (see discussion in [35]), to the extent that the study of these longer-term thermal effects themselves was neglected. Thus, the relative weight of the above-mentioned effects was not studied so far for continuous wave (CW) illumination. However, the study of the CW limit becomes interesting again, with the growing interest in thermoplasmonic applications.

In the few studies dedicated to longer-term thermal effects (i.e. for CW illumination) [36, 37], the model used for the temperature dependence of metal permittivity neglected some of the dominant physical effects, most prominently, the temperature dependence of the interband transitions. Even in the mid-infrared regime, where no intense sources are available, it did not include all dominant effects known from the literature. Thus, the quantitative predictions in these studies are questionable.

Finally, the temperature dependence of the thermal properties was not taken into account before, either for ultrafast or CW illumination to the best of our knowledge.

To close this knowledge gap, in this article, we perform a thorough theoretical study of the high-temperature regime of nanoplasmonic systems under intense optical illumination in the visible range and for CW illumination. Our study focuses on the (classical) interaction between the temperature, permittivity, and electromagnetic fields. We use experimentally measured data for the various optical and thermal properties to avoid the need to dwell on the details of the underlying physics, which, as explained, is only partially understood; however, where possible, we try to identify the relevant physical mechanisms by comparing the theory to experimental results. Specifically, we will show that the thermo-optical nonlinearity can be very strong, thus, allowing us to explain the experimental observations of the strong nonlinear scattering from metal NPs [38–41]. More generally, this study should serve as the starting point for further experimental and theoretical studies of the underlying physics, of other regime of parameters (specifically, of pulsed illumination, different materials, geometries, etc.), and enable a quantitative study of the various applications mentioned above as well as several others such as nonlinear composites/metamaterials [35, 42–44], optical limiting [45–48], plasmon lasing [49–51], and superresolution techniques based on metal NPs [6, 38–41, 52–56].

The paper is organized as follows. We start by explaining why the temperature dependence of the optical and thermal properties is usually neglected and identify cases where the temperature dependence and mutual coupling of the Maxwell and heat equations is nonnegligible. We then solve the Maxwell and heat equations self-consistently for small metal spheres illuminated by intense visible light and elucidate the large errors in the calculations of the temperature and field distributions associated with neglecting the temperature dependence of the gold permittivity both in-resonance and off-resonance. We then show that the temperature dependence of some additional parameters, such as thermal conductivity and Kapitza resistance, is also required for a correct quantitative prediction of the temperature and field distributions. Finally, we discuss the implications of our results to a previous experimental work and specify several future measurements necessary for further studies of the strong temperature nonlinearity of metals.

2 Self-consistent calculation of temperature in metal nanostructures

We want to calculate the scattering of an incident CW off some metal-dielectric nanostructure as a function of pumping intensity and/or temperature. This requires us to understand how much does the metal temperature increase under this illumination and how much, in turn, does this temperature increase affect metal permittivity (hence the electromagnetic field distribution around the nanostructure).

In the simplest model, the metal-dielectric system is assigned a single, spatially nonuniform temperature T (i.e. we neglect the difference between the electron and lattice temperatures). Then, under CW illumination (and with no temporal pump modulation), the heat equation governing the temperature dynamics reduces to the Poisson equation:

$$\nabla\cdot[\kappa(T(\vec{r}))\nabla T(\vec{r})]=-p_{\mathrm{abs}}(\vec{r};T(\vec{r})), \tag{1}$$

where κ is the thermal conductivity (specifically, κ_m and κ_{host} for the metal nanostructure and the dielectric host, respectively). Note that, in principle, thermal conductivity can be temperature dependent. The typical boundary conditions accompanying Eq. (1) are the continuity of

the temperature T and heat flux $\kappa\nabla T$ across the interface between different materials.[1]

The heat source p_{abs} represents the density of absorbed power (in units of W/cm^3). Classically, the relation between the absorbed power and the local incident electromagnetic field intensity is given by

$$p_{\text{abs}} = \frac{\epsilon_0 \omega}{2} \epsilon_m'' |\vec{E}|^2, \tag{2}$$

where $\vec{E}$ is total (local) electric field (namely, the solution of the vectorial Helmholtz equation), ω is the pump frequency, and $\epsilon_m = \epsilon_m' + i\epsilon_m''$ is the complex (relative) permittivity of the metal, which serves as the heat source in this problem. This expression is sometimes replaced by $\sim\alpha I$ (or $\sim\sigma_{\text{abs}} I$), where α is the absorption coefficient (absorption cross-section) and I is the (local) beam intensity. Quantum mechanically, p_{abs} has to be calculated as the spectral integral over all the possible transitions from electron levels and over the frequency content of the pump pulse times the respective photon energy, involving both absorption and emission to and from each level [33].

The common model in heat calculations of plasmonic systems (frequently referred to as thermoplasmonics [4]) is to solve the Maxwell equations first for ambient conditions, that is, assuming $\epsilon_m(\omega; T = T_{\text{env}})$, where T_{env} is the temperature far away from the heat-generating (metal) objects. Then, one substitutes the resulting electric field distribution into the heat source term p_{abs} (2) in the heat equation (1). Below, we refer to this approach as the temperature-independent permittivity (TIP) model.

The TIP model is appropriate as long as the relative change of the permittivity $\Delta\epsilon_m \sim \Delta T \mathrm{d}\epsilon_m/\mathrm{d}T$ is small. Typically, the thermoderivative $\mathrm{d}\epsilon_m/\mathrm{d}T$ varies between ~10^{-5}/K for standard dielectric materials [58] and up to 10^{-4}–10^{-3}/K for water [59] or metals [60, 61]. Thus, as long as the temperature increase (with respect to T_{env}) is modest (i.e. limited to a few degrees), the change of the permittivity is indeed negligible. Potentially, the opposite signs of the thermoderivatives of the dielectric material and metal may cause the overall temperature dependence of the system under consideration to be weaker than in each of the constituents [61], thus, providing further justification for treating the permittivity as temperature independent. The permittivity changes may be negligible also in the wavelength regime for which $\mathrm{d}\epsilon_m/\mathrm{d}T$ vanishes. Peculiarly, it turns out that, for gold, this regime is about 520–550 nm [60, 61] (i.e. it coincides with the plasmon resonance wavelength of small metal nanospheres, which have been subject to extensive study) [4, 31, 38–40, 61].

However, in plasmonic nanostructures under *intense* illumination (as for thermophotovoltaics [14, 15], plasmon-mediated photocatalysis [18–20], plasmon-assisted chemical vapor deposition [21], and heat-assisted magnetic recording [22]), the conditions prescribed above are typically *not* fulfilled. Indeed, whereas the (relative) modification of the *real* part of metal permittivity due to the changes of the temperature may be small, a substantial increase of the temperature (a few tens of degrees or more) may cause the *imaginary* part of metal permittivity ϵ_m'', to change *substantially*.

In the case of *external* heating (and weak illumination), one has to use the appropriate permittivity data for the ambient temperature and solve only the Maxwell equations, as done routinely for room-temperature studies. In contrast, intense (laser) illumination will result in mutual coupling of the heat and Maxwell equations via p_{abs} (2), requiring them to be solved simultaneously. In these cases, the standard model described above (TIP model), which does not take into account the thermo-optical (nonlinear) response to the electromagnetic field, would have to be replaced with a *temperature-dependent* permittivity (TDP) model. This is essential to make the results from such high temperature applications quantitatively relevant.

Remarkably, it is a common practice to take into account the thermal nonlinearities of the *host* medium (e.g. for PT imaging [5, 6, 62], cancer treatment [7], and thermal lensing [63]). However, the majority of studies within the plasmonics community *ignore* the temperature dependence of metal permittivity. Some of the earlier studies did account for the thermal response of the metal by approximating it with a cubic nonlinearity (see [25], or [26] for a more recent review). This approach was used, however, only for cases where the pump pulse was not longer than a few nanoseconds and in the perturbative regime, where the relative permittivity changes were small such that the cubic approximation is sufficient. Moreover, these studies focused primarily on the electric field distribution and ignored the temperature itself. Similarly, studies of effective medium theories applied to media with (thermal) cubic nonlinearities also focused on the field rather than the temperature distribution (see, e.g. [25, 35, 42–48, 64] and references therein). One of the reasons for that is obviously that measuring the temperature in the near field of the NPs remains a very difficult task despite the progress made recently [65, 66].

Within a TDP model, we expect to be able to distinguish between two scenarios. In the general scenario, as the temperature (hence the imaginary part of metal permittivity) changes, the heat generation rate p_{abs} changes as well. In particular, if ϵ_m'' grows with temperature, the TIP

1 However, see [57] and the discussion on Kapitza resistance below.

model will provide an *underestimation* of the actual temperature, as could be calculated from the fully coupled (TDP) model. The field distribution, on the contrary, may differ only slightly from the field distribution predicted by the simplified TIP model since typically, $\epsilon_m'' \ll |\epsilon_m'|$.

In contrast, at plasmon resonance, the metal nanostructure acts as a cavity whose quality factor scales inversely with the imaginary part of metal permittivity ϵ_m''. Accordingly, if ϵ_m'' increases with temperature, the local electric field (hence the heat power dissipation) *drops*, the resonance broadens and the overall power dissipation *decreases* with respect to the prediction of the TIP model. Accordingly, the temperature will rise more slowly, such that the simplified TIP model will provide an *overestimate* of the actual temperature. In this case, the TDP model will also predict a substantial change of the scattered field with respect to the prediction of the TIP model. The opposite will happen if ϵ_m'' decreases with temperature.

These two effects will be demonstrated analytically and numerically in Section 3. However, in the meantime, from this discussion, it is obvious that there is a strong spectral sensitivity such that the solution would almost never follow the predictions of the TIP model. Below, we demonstrate the differences between the TIP and TDP models in some specific examples, showing that they can be substantial for realistic cases and for many applications that are studied extensively these days.

To quantify these differences, one has to have available comprehensive data of the temperature dependence of metal permittivity. However, quite surprisingly, such data hardly exist, even for gold, which is the plasmonic material studied most extensively (see detailed discussion in [67]). In the absence of elaborate experimental data, theoretical models for the temperature dynamics [27, 32, 68] and metal permittivity dynamics [31] were developed. However, as mentioned above, effectively all these studies focused on the *ultrafast* (up to a few picoseconds) regime, and only a few of these studies accounted for all the relevant physical mechanisms [31]. Similarly, the multitude of models where the thermal response is approximated as a cubic nonlinearity [25, 26] did not consider the thermal response on time scales longer than a few nanoseconds. The quantitative predictions in the few studies of the CW nonlinear response should, as mentioned, be taken with a grain of salt due to the missing ingredients in the permittivity models employed.

Thus, to the best of our knowledge, there is no complete model for the *slow* thermal response as appropriate for CW illumination. In this regime, the electronic response that dominates the ultrafast response becomes negligible, and other effects, such as lattice heating and thermal expansion [31], stress and strain, band shifting [69], and indirect (i.e. phonon-assisted) interband transitions [70], take dominance.

To close this knowledge gap, we have recently performed ellipsometry measurements to retrieve the permittivity data of bulk gold at increasing temperatures [67]. Our study showed that ϵ_m'' increases substantially with temperature across the visible spectral range. Indeed, in the temperature regime of 300–570 K, Figure 1 shows changes of up to ~25%–30% in the visible range for selected wavelengths. In the near-infrared regime, an increasingly stronger dependence on temperature is observed [67].

Our study also shows that the changes to the real part of the gold permittivity are substantially smaller with respect to the room temperature values (about 1%–3% in the temperature regime studied here). Similar results appear in two recent independent studies [71, 72] as well as for Ag [71, 73].

To simplify the modeling and discussion, we assume in what follows that the host (dielectric) material permittivity is purely real and nondispersive. This assumption has a negligible effect on our results. Indeed, the numerical examples below show that the changes of the host permittivity and of the real part of metal permittivity have a secondary effect on the temperature and field distribution. This residual temperature dependence will have to be taken into account in applications of PT imaging [5, 6, 62] and treatment [7], water boiling [11, 12], plasmonic (thermo)photovoltaics [14, 15], thermal lensing

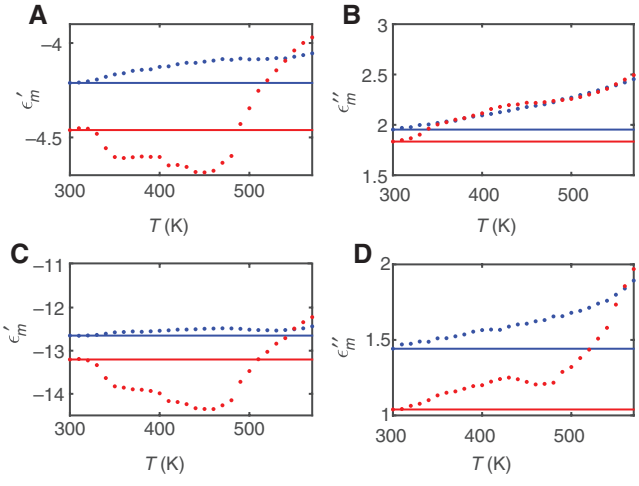

Figure 1: Au ellipsometry data.
(A) Real and (B) imaginary parts of the (relative) permittivity extracted from the ellipsometry measurements of an annealed (blue) and unannealed (red) Au film at $\lambda = 533$ nm for 300–570 K. (C and D) Same data for $\lambda = 671$ nm.

[63], and plasmon-assisted catalysis [18–20], where the level of temperature rise of the surrounding medium is critical. This is, however, left for future studies.

3 Metal spheres

Although, in general, the problem at hand requires a self-consistent numerical iteration scheme involving both the Maxwell and heat equations [36, 37], for some simple geometries, one can avoid solving the Maxwell equations and rely on known solutions. As a generic example, we now consider the temperature of a single small (with radius $a \ll \lambda$) spherical metal NP illuminated by a plane wave. Hence, the quasi-electrostatic solution of Maxwell equations [74] holds such that the electric field inside the NP ($\vec{E}_{\rm NP} \equiv \vec{E}(r<a)$) is uniform and given by

$$\vec{E}_{\rm NP} = \frac{3\epsilon_d}{\epsilon_m(\omega;\, T)+2\epsilon_d}\vec{E}_{\rm inc}, \tag{3}$$

where $\vec{E}_{\rm inc}$ is uniform (i.e. a fixed parameter). In what follows, we suppress the vector symbol. Using Eq. (3) in Eq. (2) gives a uniform power dissipation:

$$p_{\rm abs}(\omega,\, T(r<a)) = \frac{\epsilon_0\omega}{2}\epsilon_m''(T)\left|\frac{3\epsilon_d}{\epsilon_m(T)+2\epsilon_d}\right|^2 |E_{\rm inc}|^2. \tag{4}$$

The solution of the Poisson equation (1) for this case is [4]

$$T(r) = T_{\rm env} + \begin{cases} \dfrac{P_{\rm abs}(\omega,\, T)}{4\pi\kappa_{\rm host}a}\left[1+\dfrac{\kappa_{\rm host}}{2\kappa_m}\left(1-\dfrac{r^2}{a^2}\right)\right], & r<a, \\ \dfrac{P_{\rm abs}(\omega,\, T)}{4\pi\kappa_{\rm host}r}, & r>a, \end{cases} \tag{5}$$

where κ_m and $\kappa_{\rm host}$, the thermal conductivities of the NP and host, respectively, are assumed for the moment to be temperature independent (hence uniform) and $P_{\rm abs}(\omega,\, T) \equiv \int p_{\rm abs}\,{\rm d}V$ is the total power dissipated in the NP.

Because typically $\kappa_m \gg \kappa_{\rm host}$, it follows from Eq. (5) that heat diffusion is sufficiently strong to homogenize the temperature within the NP; this assumption is supported by exact simulations, showing temperature uniformity even for much larger NPs [37]. Thus, neglecting the small temperature variation, we can define $T_{\rm NP} \equiv T(r<a)$ so that $P_{\rm abs} = 4\pi a^3 p_{\rm abs}/3$; by Eq. (5), we then get

$$T_{\rm NP} = T_{\rm env} + \frac{a^2}{3\kappa_{\rm host}}p_{\rm abs}(T_{\rm NP}). \tag{6}$$

Substituting Eq. (4) in Eq. (6) gives

$$T_{\rm NP} = T_{\rm env} + \frac{\epsilon_0\omega}{2}\frac{3a^2}{\kappa_{\rm host}}|E_{\rm inc}|^2\frac{\epsilon_d^2}{|\epsilon_{\rm tot}'+\epsilon_m''(T_{\rm NP})|^2}\epsilon_m''(T_{\rm NP}), \tag{7}$$

where $\epsilon_{\rm tot}' \equiv \epsilon_m' + 2\epsilon_d$.

Equation (7) is a simple root equation for the NP temperature that is easy to solve. However, before presenting detailed numerical examples, we discuss several general properties of the solution.

In the general (off-resonance) case, the real parts of the permittivities do not perfectly cancel, such that, typically, $\epsilon_{\rm tot}' \gg \epsilon_m''$. Then, we get

$$T_{\rm NP} \approx T_{\rm env} + \frac{\epsilon_0\omega}{2}\frac{3a^2}{\kappa_{\rm host}}|E_{\rm inc}|^2\frac{\epsilon_d^2}{|\epsilon_{\rm tot}'|^2}\epsilon_m''(T_{\rm NP}). \tag{8}$$

Indeed, as predicted, we see from Eq. (8) that the absorbed power (hence the overall temperature) will be *higher* in the TDP model compared to the TIP model.

On the contrary, at resonance, the real part of the denominator vanishes such that upon a temperature increase, the power dissipation (4) drops for increasing ϵ_m''. This is due to the resonant nature of the interaction – ϵ_m'' is inversely proportional to the quality factor of this effective resonator. At the same time, the resonance broadens and the temperature itself is given by

$$T_{\rm NP} = T_{\rm env} + \frac{\epsilon_0\omega}{2}\frac{3a^2}{\kappa_{\rm host}}|E_{\rm inc}|^2\frac{\epsilon_d^2}{\epsilon_m''(T_{\rm NP})}. \tag{9}$$

We thus see from Eq. (9) that at resonance the absorbed power (hence the overall temperature) will be *lower* in the TDP model compared to the TIP model.

From the above discussion, the reasons for neglecting the changes of the real part of the metal (and dielectric) permittivities become apparent. Indeed, the changes of $\epsilon_{\rm tot}'$ are relatively small and cause only a slight shift of the plasmon resonance position. It is clear, however, that the important parameter is the shift of the real part of $\epsilon_{\rm tot}'$ rather than the shift of any of its constituents, as various combinations of thermoderivatives of the metal and dielectric will give rise to shifts in different directions.

Once the NP temperature is determined, one can calculate the scattered field using the quasi-static solution [74]. In the case of a single intense (pump) beam, the scattered field $\vec{E}_{sc} \equiv \vec{E}(r>a) - \vec{E}_{\rm inc}$, is given by

$$\vec{E}_{sc}(\omega_{\rm pump},\, T_{\rm NP}) = \frac{\epsilon_d - \epsilon_m(\omega_{\rm pump},\, T_{\rm NP})}{\epsilon_{\rm tot}' + i\epsilon_m''(\omega_{\rm pump},\, T_{\rm NP})}\frac{a^3}{r^3}|E_{\rm inc}(\omega_{\rm pump})|(2\cos\theta\hat{r}+\sin\theta\hat{\theta}). \tag{10}$$

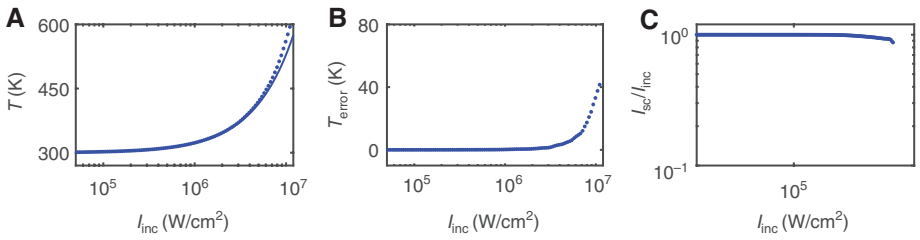

Figure 2: Temperature and intensity for intense off-resonant illumination.
(A) Calculated temperature for $\lambda = 533$ nm and the off-resonance case ($\epsilon_d = 5.5$) for the TDP model (blue dots) and TIP model (solid blue line) based on annealed permittivity data. (B) Temperature difference between both models. (C) Peak intensity of the scattered field as a function of the incoming pump intensity for the two models.

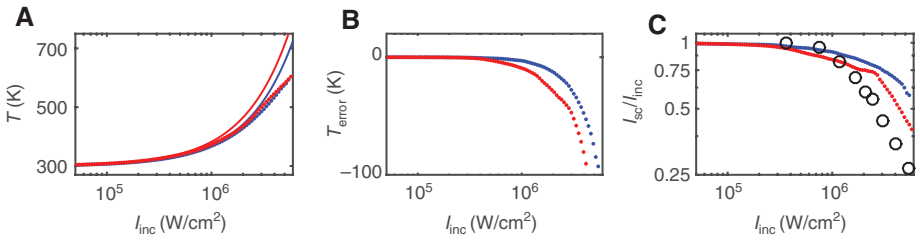

Figure 3: Temperature and intensity for intense on-resonant illumination.
Same as in Figure 2 for the on-resonance case (obtained by setting $\epsilon_d = 2.25$). Also shown in (a) are the results for unannealed data (TDP model, red dots; TIP model, solid red line), and (b) shows the corresponding difference between the two models. Finally, (c) shows also the (normalized) experimentally measured data of scattering from a single 40 nm Au NP embedded in index matching oil under CW illumination.

When the intense beam is accompanied by a second, weaker (probe) beam, the scattering of the probe will be given by the same expression, where the permittivities and fields are evaluated at the probe frequency. Because this case is effectively similar to the standard linear case or to the case of external heating [67, 75], it will not be considered further.

3.1 Numerical examples

Based on the experimental data for annealed gold [67], as appropriate for metal NPs made by the pulsed laser ablation of gold films [76], we initially solve Eq. (7) for $\lambda = 533$ nm (permittivity data given in Figure 1A and B). Figure 2A and B shows that, when the system is tuned away from resonance (the host permittivity is $\epsilon_{\text{host}} = 5.5$), for sufficiently large pumping intensity, the naive (TIP) model indeed *underestimates* the temperature rise in the particle. For example, we see that the TDP model predicts $T = 594$ K, whereas the TIP gives $T = 552$ K (i.e. an error of ~17% of the temperature increase). This error is commensurate with the corresponding change of ϵ_m'', which increased by ~30% (the real part changes by ~1%). Nevertheless, the TIP model still predicts the scattered field with reasonable accuracy (Figure 2C). Indeed, in this case, the denominator for the expression for the scattering [see Eq. (10)] is only slightly affected by the change of the imaginary part of the permittivity.

At resonance, on the contrary ($\lambda = 533$ nm but with $\epsilon_d = 2.25$), the naive (TIP) model *overestimates* the temperature rise in the NP (see Figure 3A and B). For example, when the TDP model predicts $T = 594$ K, the TIP gives $T = 694$ K (i.e. ~34% error in temperature rise measurement). More importantly, in this case, the TDP model predicts a 40% decrease of the scattering (Figure 3C). Figure 3 also shows the results based on nonannealed permittivity data as appropriate for metal NPs synthesized in solution [67]. One can see that, although the results are qualitatively similar, the nonannealed gold shows a much stronger sensitivity to the rising temperature. This emphasizes the need to account for the relevant permittivity data depending on the metal particle preparation method [67].

Most importantly, Figure 3C also shows a comparison to measured scattering data[2] from a single 40 nm Au NP embedded in index matching oil under CW illumination. One clearly observes very good qualitative agreement between the theory and the measurement, achieved without any fitting parameters. This agreement between the scattered fields also reveals the NP temperature – the lowest scattering levels are attained for a temperature rise

2 See discussion of the experimental set-up in [39].

of only a few hundred degrees (i.e. well below the melting temperature of the Au NPs), which is somewhat less than 1000 K [13]. Note that a quantitative agreement of the scattered field and temperature requires a further refinement of our modeling (see Section 5).

As a comparison, we show in Figure 4 the temperature and scattered field for resonant illumination at $\lambda = 671$ nm ($\epsilon_d = 2.5$); the permittivity data at this wavelength are shown in Figure 1C and D. Although the trends are qualitatively similar to the case of $\lambda = 533$ nm, the nonlinear response is stronger – the scattered field drops by 60% and the temperature error is up to ~250 K.

Finally, we note that, when the variation of the real part with temperature is taken into account [i.e. when we solve Eqs. (7) and (10) for $\epsilon'_{\text{tot}}(T) \neq 0$], there is no substantial change of any of the results described so far. This happens because the (absolute, as well as) relative changes of the real part of metal permittivity with temperature are typically smaller than those of the imaginary part; accordingly, they have far smaller influence on the temperature and scattering.

4 Additional considerations

Below, we discuss two additional aspects of the thermo-optical problem at hand that, to the best of our knowledge, are discussed for the first time in the current context.

4.1 Role of the temperature dependence of thermal conductivity

So far, we assumed that the thermal conductivities are temperature independent. However, the temperature dependence of the thermal conductivity is well known for a wide range of materials. Remarkably, its variation with temperature is comparable to that of metal permittivity. For example, the thermal conductivity of water increases by about 10% between 300 and 400 K; beyond this temperature, the water boils. Oil exhibits comparable changes over a wider temperature range, with some oils exhibiting increased conductivity with growing temperature and some exhibiting reduced conductivity. The thermal conductivity of other materials, such as collagen [77], quartz, silicon wires, or aluminum oxide, exhibit even stronger temperature dependence. The thermal conductivity of the metal itself also varies substantially with the temperature; however, because it is typically much larger than the host conductivity, this variation plays a negligible role for our purposes [see Eq. (5)]. Thus, it is clear that this dependence has to be taken into account to accurately determine the temperature and field distributions. In general, if the host thermal conductivity increases with temperature, then the temperature rise is lower than that predicted by a model that ignores this effect and vice versa.

The exact solution (5) used so far will not hold anymore for a temperature (hence space)-dependent thermal conductivity. However, exploiting again the uniformity of the temperature inside the NP allows us to keep using the implicit relation (7). Numerical simulations (see Figure 5) show that the error associated with the change of thermal conductivity with the temperature (taken as $T_{\text{env}}/\kappa_{\text{env}}\mathrm{d}\kappa/\mathrm{d}T \sim \pm 10\%$) is of the same order of the temperature change itself. As expected, a similar trend is found also for the off-resonant case (not shown).

4.2 Role of the interface (Kapitza) conductivity

A more realistic model of the heat transfer between the NP and its surrounding has to account for the finite interface (Kapitza) conductivity g [13, 24, 78]. In this case, it was shown [57] that the solution for the illuminated sphere is modified only inside the sphere, namely,

$$T_{\text{NP}} = \frac{P_{\text{abs}}(\omega)}{4\pi a}\left[\frac{1}{\kappa_{\text{host}}} + \frac{1}{ga}\right], \tag{11}$$

where, for simplicity, we again assumed a uniform temperature inside the NP. The finiteness of the interface

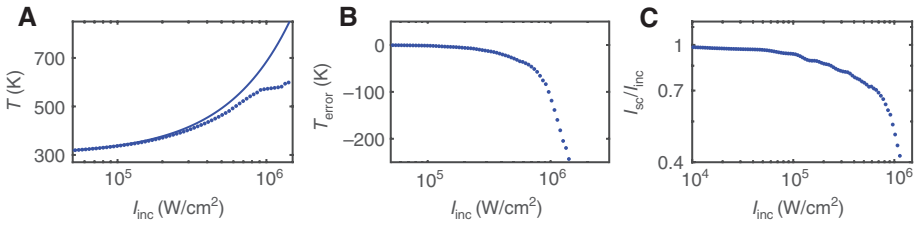

Figure 4: Temperature and intensity for intense on-resonant illumination ($\lambda = 671$ nm). Same as in Figure 2 for the on-resonance case ($\lambda = 671$ nm and $\epsilon_d = 2.5$).

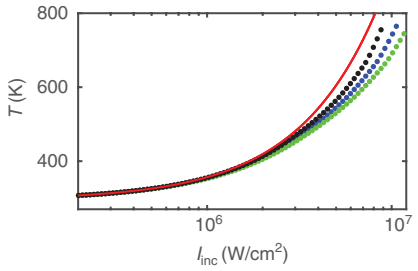

Figure 5: Effect of the temperature dependence of the host thermal conductivity on NP temperature.
Calculated temperature for on-resonance case ($\lambda = 533$ nm) for the TIP model (solid red line) and TDP model with temperature-independent thermal conductivity (blue dots), both as in Figure 3, compared to a thermal conductivity that increases with temperature (green dots) and thermal conductivity that decreases with temperature (black dots). In the latter two cases, thermal conductivity changes by as much as 13%.

Kapitza conductivity means that the generated power within the NP escapes more slowly; hence, the overall NP temperature is higher (with respect to the case of infinite interface conductivity).

In general, the value of interface Kapitza conductivity is known only for a select few cases – its calculation requires heavy and somewhat ambiguous molecular dynamics simulations (see e.g. [13] for a discussion) and its measurement is a tough task. However, fortunately, it turns out that gold nanostructures were some of the few cases that were studied. A fit to experimental results performed in [61] yielded $g \sim 110$ MW/m^2 K for the interface between a 18 nm gold sphere and water. With this value, the correction in Eq. (11) with respect to the case of infinite interface conductivity is $\kappa_{\text{host}}/ga = 33$ nm/a. Thus, for the small particles under consideration here, this term is clearly far from being negligible. A similar procedure for gold-ethanol interface yielded $g \sim 40$ MW/m^2 K (i.e. again, providing a substantial contribution). Similar values were reported for the Kapitza conductance between gold and silicon under various surface treatments at temperatures below room temperature [79].

If Kapitza conductivity was studied in only a limited number of papers, then its temperature dependence was studied even less. Molecular dynamics calculations performed in [13] for 3 nm gold NPs yielded $g \sim 180$ MW/m^2 K and a temperature dependence similar to that of permittivity and thermal conductivity [i.e. a variation by more than 10% for the temperature range covered in the current manuscript (300–800 K)]. This temperature dependence has a similar effect to that of thermal conductivity – an increasing conductance with temperature will give rise to lower temperatures compared to models that ignore it.

5 Discussion

The results shown above raise a clear need to take into account the temperature dependence of the optical and thermal properties of the metal (and its surroundings) in calculations of field and temperature under intense illumination conditions. In particular, the errors associated with the neglect of the temperature dependence of these quantities grow monotonically with the temperature rise and can reach several tens or even hundreds of degrees for the refractory applications (i.e. even up to 100% relative errors); for resonant illumination, there are comparable relative errors in the scattered fields. In fact, for some applications, such as PT imaging [5, 6, 62], correcting errors of even a few percent could be substantial.

More generally, our calculations provide a complete treatment of nonlinear plasmonic systems at the high-temperature regime that goes beyond the perturbative description of the thermo-optical response [25, 26, 60]. Indeed, we intentionally avoid any assumption on the functional dependence of the metal permittivity on the temperature or intensity (e.g. an assumption of a cubic nonlinear response [25], of a constant thermoderivative $\mathrm{d}\epsilon_m/\mathrm{d}T$ [44, 60], or of an averaged response in the effective medium spirit [44]). This approach allowed us to identify the thermo-optical mechanism as being responsible for the nonlinear scattering of monochromatic waves from Au NPs that was observed experimentally [38–41], showing deviations from the linear prediction (TIP) of several tens of percent (see Figure 3). Indeed, such changes of scattering are shown to be commensurate with the change of the imaginary part of metal permittivity with the temperature (see Figure 1). Remarkably, we confirm that the effect occurs on a subwavelength scale, from a *single* NP and potentially its immediate surrounding (via the thermal conductivity), rather than being an effect accumulated on macroscopic distances or due to interparticle interactions or aggregation, as one may conclude from previous studies of NP suspensions (see, e.g. [43, 45–48, 80]).

In contrast to previous works, which relied on a theoretical model that missed some dominant physical effects [36, 37, 75], our study relies on *experimentally-measured* permittivity data [67] and focuses on the visible range. Furthermore, we show stronger effects from NPs smaller than those studied before. Yet, it is important to note that our model provides only a *qualitative* match to the experimental data. A quantitative agreement requires accounting for the actual size of the particles (i.e. to go beyond the quasi-static approximation employed here, as done in [37]) and for the temperature dependence of the thermal properties of the metal and host, which is currently not

known. For completeness, it is also desired to develop a theoretical model for the (slow) thermal nonlinearity of gold to support the experimental results. In contrast to the common models (used in some previous studies [36, 37, 75]), a complete theoretical model will have to account for the temperature dependence of metal permittivity on both intraband *and interband* transitions and specifically for the effects of the temperature on the NP volume, electron scattering rates, electron distribution (Fermi smearing), lattice spacing (band shifting), and stress/strain build-up, as well as for nonequilibrium effects and multiphoton absorption, which we neglected. A model that describes the interplay and relative importance of these effects is yet to be developed. Such a model will be also particularly important to explain the nonlinear scattering under *pulsed* illumination, which typically involves higher intensities than for CW (up to GW/cm^2), and exhibited *opposite* trends to those observed for CW illumination [45–48, 80].

In the same vein, we should mention that the current analysis of the thermal effects may not be sufficient to address the complete intensity dependence of the scattering from metal NPs. Indeed, it was shown [38, 40] that, for sufficiently high excitation intensities, the decrease of the scattering changes to a sharp increase, occasionally and somewhat confusingly, referred to as "reverse saturation".[3] This effect may be related to electron population redistribution due to Fermi smearing (i.e. based on the distribution of thermalized electrons), which shows a rather complicated and nonintuitive spectral dependence with several spectral regimes where the permittivity decreases upon heating [28–31]. Alternatively, the increased scattering may be related to absorption saturation (i.e. based on the distribution of *nonthermal* electrons) [25, 33] or to an effect associated with the host [e.g. (nonlinear) absorption and phase/structural change]. The determination of its origin also awaits the comprehensive permittivity model and thus left for a future study.

In that regard, we emphasize that the use of the permittivity data under external heating in laser illumination calculations (as adopted in the current study or in [31]) is justified only if the effects associated with nonthermal electrons, which accompany intense illumination, are negligible compared to the effects associated with thermalized electrons. This seems to be the case for gold [26] – the absorption saturation due to interband transitions, which is related to partial population inversion, is predicted [25] and experimentally verified [43, 64] to be smaller than the nonlinearity associated with heating (thermalized electrons, Fermi smearing) at least for moderately high intensities and pulsed illumination. A simple estimate based on the measured cubic nonlinearity, $\chi^{(3)\prime\prime}_{\mathrm{Au}} \sim 5\cdot 10^{-9}\,\mathrm{cm}^2/\mathrm{W}$ at $\lambda = 532$ nm [25, 43, 64], together with the associated field enhancement within the gold, $|3\epsilon_d/\epsilon''_m|^2 \sim 20$ (see Eq. (3) and [81]), shows that the permittivity change for $I_{\mathrm{inc}} = 1\,\mathrm{MW/cm}^2$ induces a ~10% change of the imaginary part of the permittivity, as indeed we have observed experimentally (see Figures 1 and 3).[4]

Having said that, we emphasize that the estimates above, which are based on the measurements of the *ultrafast* thermal response, are only partially appropriate for the current context of a CW illumination. Indeed, the ultrafast thermal nonlinearity was derived in [25] by neglecting the diffusion of heat from the NP to its surroundings (see also [58]). In our configuration, however, heat diffusion is clearly important [see, e.g. Eq. (7)], so that the overall thermal response depends also on the host properties as well as on the particle size. This may give rise to different values of the nonlinearity. In general, though, as already noted above, a complete quantitative match of the model to the experimental data will have to be deferred to a future study.

Finally, we hope that our study would motivate further studies of thermo-optical nonlinearities at the high-temperature regime of other gold NPs as well as similar studies of other metals, especially those proposed for use in refractory plasmonics applications [22].

Acknowledgments: We would like to thank P.-T. Shen, I. Gurwich, M. Spector, and Y. Dubi for many useful discussions. Y. Sivan acknowledges the financial support from the People Programme (Marie Curie Actions) of the European Union's Seventh Framework Programme (FP7/2007-2013) under REA grant agreement no. 333790 and support from a Israel National Nanotechnology Initiative. S.W. Chu acknowledges the financial support

3 This nomenclature was adopted due to the reminiscence of the absorption/scattering data to that obtained from some atoms or molecules.

4 This implies specifically that the arguments used in [39] to explain the scaling of the deviation point of the scattering curve from the linear prediction were *incorrect*. This error originated from the use of the macroscopic absorption cross-section (of the NP) rather than the atomistic cross-section in the estimate of the relaxation time as appropriate for a single atom effect. Indeed, as the relaxation time in metals is several orders of magnitude faster than in semiconductors, one can expect the saturation levels to be correspondingly higher. Yet, the scaling of the onset of the nonlinear effect is surely a valid experimental observation and is explained in the current context by the thermal effect, which indeed scales with the absorption cross-section of the NP itself [see discussion under Eq. (2)].

from the Ministry of Science and Technology (Taiwan) under grants number MOST 101-2923-M-002-001-MY3 and MOST-102-2112-M-002-018-MY3.

References

[1] Schuller J, Barnard E, Cai W, Jun Y, White J, Brongersma M. Plasmonics for extreme light concentration and manipulation. Nat Mater 2010;9:193.

[2] Barnes W. Metallic metamaterials and plasmonics. Philos Trans A Math Phys Eng Sci 2011;369:3431–3.

[3] Govorov A, Richardson H. Generating heat with metal nanoparticles. Opt Express 2007;2:30–8.

[4] Baffou G, Quidant R. Thermo-plasmonics: using metallic nanostructures as nano-sources of heat. Laser Photon Rev 2013;7:171–87.

[5] Boyer D, Tamarat P, Maali A, Lounis B, Orrit M. Photothermal imaging of nanometer-sized metal particles among scatterers. Science 2002;297:1160–3.

[6] Zharov V, Lapotko D. Photothermal imaging of nanoparticles and cells. IEEE J Sel Top Quant Electron 2005;11:733–51.

[7] Dewhirst M, Viglianti B, Lora-Michiels M, Hanson M, Hoopes P. Basic principles of thermal dosimetry and thermal thresholds for tissue damage from hyperthermia. Int J Hyperthermia 2003;19:267–94.

[8] Desiatov B, Goykhman I, Levy U. Direct temperature mapping of nanoscale plasmonic device. Nano Lett 2014;14:648–52.

[9] Atwater H, Polman A. Plasmonics for improved photovoltaic devices. Nat Mater 2010;9:205–13.

[10] Baffou G, Polleux J, Rigneault H, Monneret S. Super-heating and micro-bubble generation around plasmonic nanoparticles under CW illumination. J Phys Chem C 2014;118, 4890–8.

[11] Neumann O, Urban A, Day J, Lal S, Nordlander P, Halas N. Solar vapor generation enabled by nanoparticles. ACS Nano 2013;7:42–9.

[12] Fang Z, Zhen Y, Neumann O, Polman A, de Abajo FG, Nordlander P, Halas N. Evolution of light-induced vapor generation at a liquid-immersed metallic nanoparticle. Nano Lett 2013; 13:1736–42.

[13] Chen X, Munjiza A, Zhang K, Wen D. Molecular dynamics simulation of heat transfer from a gold nanoparticle to a water pool. J Phys Chem C 2014;118:1285–93.

[14] Molesky S, Dewalt C, Jacob Z. High temperature epsilon-near-zero and epsilon-near-pole metamaterial emitters for thermophotovoltaics. Opt Express 2013;21:A96–110.

[15] Liu J, Guler U, Lagutchev A, Kildishev A, Malis O, Boltasseva A, Shalaev V. Quasi-coherent thermal emitter based on refractory plasmonic materials. Opt Mater Express 2014;5:2721–8.

[16] Khurgin J, Sun G, Chen W, Tsai W-Y, Tsai D. Ultrafast thermal nonlinearity. Sci Rep 2015;5:17899.

[17] Rousseau E, Siria A, Jourdan G, Volz S, Comin F, Chevrier J, Greffet J-J. Radiative heat transfer at the nanoscale. Nat Photon 2009;3:514–7.

[18] Linic S, Christopher P, Ingram D. Plasmonic-metal nanostructures for efficient conversion of solar to chemical energy. Nat Mater 2011;10:911–21.

[19] Zhou X, Liu G, Yu J, Fan W. Surface plasmon resonance-mediated photocatalysis by noble metal-based composites under visible light. J Mater Chem 2012;22:21337–54.

[20] Clavero C. Plasmon-induced hot-electron generation at nanoparticle/metal-oxide interfaces for photovoltaic and photocatalytic devices. Nat Photon 2014;8:95–103.

[21] Boyd D, Greengard L, Brongersma M, El-Naggar M, Goodwin D. Plasmon-assisted chemical vapor deposition. Nano Lett 2006;6:2592–7.

[22] Guler U, Boltasseva A, Shalaev V. Refractory plasmonics. Science 2014;334:263.

[23] Rodriguez A, Ilic O, Bermel P, Celanovic I, Joannopoulos J, Soljačić M, Johnson S. Frequency-selective near-field radiative heat transfer between photonic crystal slabs: a computational approach for arbitrary geometries and materials. Phys Rev Lett 2011;107:114302.

[24] Merabia S, Shenogin S, Joly L, Keblinski P, Barrata J-L. Heat transfer from nanoparticles: a corresponding state analysis. Proc Natl Acad Sci USA 2009;106:15113–8.

[25] Hache F, Ricard D, Flytzanis C, Kreibig U. The optical Kerr effect in small metal particles and metal colloids: the case of gold. Appl Phys A 1988;47:347.

[26] Boyd R, Shi Z, Leon ID. The third-order nonlinear optical susceptibility of gold. Opt Commun 2014;326:74–9.

[27] Anisimov S, Kapeilovich B, Perelman T. Electron emission from metal surfaces exposed to ultrashort laser pulses. Sov Phys JETP 1974;39:375–8.

[28] Guerrisi M, Rosei R, Winsemius P. Splitting of the interband absorption edge in Au. Phys Rev B 1975;12:557–63.

[29] Winsemius P, Guerrisi M, Rosei R. Splitting of the interband absorption edge in Au: temperature dependence. Phys Rev B 1975;12:4570.

[30] Rosei R, Lynch D. Thermomodulation spectra of Al, Au, and Cu. Phys Rev B 1972;5:3883.

[31] Stoll T, Maioli P, Crut A, Fatti ND, Vallée F. Advances in femto-nano-optics: ultrafast nonlinearity of metal nanoparticles. Eur Phys J B 2014;87:260.

[32] Groeneveld R, Sprik R, Lagendijk A. Femtosecond spectroscopy of electron-electron and electron-phonon energy relaxation in Ag and Au. Phys Rev B 1995;51:11433–45.

[33] Kornbluth M, Nitzan A, Seidman T. Light-induced electronic non-equilibrium in plasmonic particles. J Chem Phys 2013;138:174707.

[34] Brown A, Sundararaman R, Narang P, Goddard W, Atwater H. Nonradiative plasmon decay and hot carrier dynamics: effects of phonons, surfaces, and geometry. ACS Nano 2016;10:957–66.

[35] Hamanaka Y, Nakamura A, Hayashi N, Omi S. Dispersion curves of complex third-order optical susceptibilities around the surface plasmon resonance in Ag nanocrystal-glass composites. J Opt Soc Am B 2003;20:1227–32.

[36] Alabastri A, Tuccio S, Giugni A, Toma A, Liberale C, Das G, Angelis FD, di Fabrizio E, Zaccaria R. Molding of plasmonic resonances in metallic nanostructures: dependence of the nonlinear electric permittivity on system size and temperature. Materials 2013;6:4879–910.

[37] Alabastri A, Toma A, Malerba M, Angelis FD, Zaccaria R. High temperature nanoplasmonics: the key role of nonlinear effects. ACS Photon 2015;2:115–20.

[38] Chu S-W, Wu H-Y, Huang Y-T, Su T-Y, Lee H, Yonemaru Y, Yamanaka M, Oketani R, Kawata S, Fujita K. Saturation and

reverse saturation of scattering in a single plasmonic nanoparticle. ACS Photon 2013;1:32–7.
[39] Chu S-W, Su T-Y, Oketani R, Huang Y-T, Wu H-Y, Yonemaru Y, Yamanaka M, Lee H, Zhuo G-Y, Lee M-Y, Kawata S, Fujita K. Measurement of a saturated emission of optical radiation from gold nanoparticles: application to an ultrahigh resolution microscope. Phys Rev Lett 2014;112:017402.
[40] Lee H, Oketani R, Huang Y-T, Li K-Y, Yonemaru Y, Yamanaka M, Kawata S, Fujita K, Chu S-W. Point spread function analysis with saturable and reverse saturable scattering. Opt Express 2014;22:26016–22.
[41] Wu H-Y, Huang Y-T, Shen P-T, Lee H, Oketani R, Yonemaru Y, Yamanaka M, Shoji S, Lin K-H, Chang C-W, Kawata S, Fujita K, Chu S-W. Ultrasmall all-optical plasmonic switch and its application to superresolution imaging. Sci Rep 2016;6:24293.
[42] Smith D, Fischer G, Boyd R, Gregory D. Cancellation of photoinduced absorption in metal nanoparticle composites through a counterintuitive consequence of local field effects. J Opt Soc Am B 1997;14:1625.
[43] Liao H, Xiao R, Fu J, Wang H, Wong K, Wong G. Origin of third-order optical nonlinearity in au:sio2 composite films on femtosecond and picosecond time scales. Opt Lett 1998;23:388.
[44] Rashidi-Huyeh M, Palpant B. Counterintuitive thermo-optical response of metal-dielectric nanocomposite materials as a result of local electromagnetic field enhancement. Phys Rev B 2006;74:075405.
[45] Elim H, Yang J, Lee J-Y, Mi J, Ji W. Observation of saturable and reverse-saturable absorption at longitudinal surface plasmon resonance in gold nanorods. Appl Phys Lett 2006;88:083107.
[46] Gurudas U, Brooks E, Bubb D, Heiroth S, Lippert T, Wokaun A. Saturable and reverse saturable absorption in silver nanodots at 532 nm using picosecond laser pulses. J Appl Phys 2008;104:073107.
[47] West R, Wang Y, Goodson T. Nonlinear absorption properties in novel gold nanostructured topologies. J Phys Chem B 2003;107:3419–26.
[48] Dengler S, Kübel C, Schwenke A, Ritt G, Eberle B. Near- and off-resonant optical limiting properties of gold-silver alloy nanoparticles for intense nanosecond laser pulses. J Opt 2012;14:075203.
[49] Oulton R, Sorger V, Zentgraf T, Ma R-M, Gladden C, Dai L, Bartal G, Zhang X. Plasmon lasers at deep subwavelength scale. Nature 2009;461:629–32.
[50] Sivan Y, Xiao S, Chettiar U, Kildishev A, Shalaev V. Frequency-domain simulations of a negative-index material with embedded gain. Opt Express 2009;17:24060.
[51] Xiao S, Drachev V, Kildishev A, Ni X, Chettiar U, Yuan H-K, Shalaev V. Loss-free and active optical negative-index metamaterials. Nature 2010;466:735–8.
[52] Zharov V. Ultrasharp nonlinear photothermal and photoacoustic resonances and holes beyond the spectral limit. Nat Photon 2011;5:110–6.
[53] Sivan Y, Sonnefraud Y, Kéna-Cohen S, Pendry J, Maier S. Nanoparticle-assisted stimulated emission depletion nanoscopy. ACS Nano 2012;6:5291–6.
[54] Sivan Y. Performance improvement in nanoparticle-assisted stimulated emission depletion nanoscopy. Appl Phys Lett 2012;101:021111.
[55] Balzarotti F, Stefani F. Plasmonics meets far-field optical nanoscopy. ACS Nano 2012;6:4580.
[56] Sonnefraud Y, Sinclair H, Sivan Y, Foreman M, Dunsby C, Neil M, French P, Maier S. Experimental proof of concept of nanoparticle-assisted STED. Nano Lett 2014;14:4449–53.
[57] Baffou G, Rigneault H. Femtosecond-pulsed optical heating of gold nanoparticles. Phys Rev B 2011;84:035415.
[58] Boyd R. Nonlinear optics. 2nd ed. , London, Academic Press, 2003.
[59] Blum O, Shaked N. Prediction of photothermal phase signatures from arbitrary plasmonic nanoparticles and experimental verification. Light Sci Appl 2015;4:322.
[60] Wilson R, Apgar B, Martin L, Cahill D. Thermoreflectance of metal transducers for optical pump-probe studies of thermal properties. Opt Express 2012;20:28829–38.
[61] Stoll T, Maioli P, Crut A, Rodal-Cedeira S, Pastoriza-Santos I, Vallée F, Fatti ND. Time-resolved investigations of the cooling dynamics of metal nanoparticles: impact of environment. J Phys Chem C 2015;119:12757–64.
[62] Danielli A, Maslov K, Garcia-Uribe A, Winkler A, Li C, Wang L, Chen Y, Dorn G, Wang L. Label-free photoacoustic nanoscopy. J Biomed Opt 2014;19:086006.
[63] Donner J, Morales-Dalmau J, Aldaa I, Marty R, Quidant R. Fast and transparent adaptive lens based on plasmonic heating. ACS Photon 2015;2:355–60.
[64] Smith D, Yoon Y, Boyd R, Campbell J, Baker L, Crooks R, George M. Z-scan measurement of the nonlinear absorption of a thin gold film. J Appl Phys 1999;86:6200.
[65] Honda M, Saito Y, Smith N, Fujita K, Kawata S. Nanoscale heating of laser irradiated single gold nanoparticles in liquid. Opt Express 2011;19:12375–83.
[66] Tzeng Y-K, Tsai P-C, Liu H-Y, Chen O, Hsu H, Yee F-G, Chang M-S, Chang H-C. Time-resolved luminescence nanothermometry with nitrogen-vacancy centers in nanodiamonds. Nano Lett 2015;15:3945–52.
[67] Shen P-T, Sivan Y, Lin C-W, Liu H-L, Chang C-W, Chu S-W. Temperature-dependent permittivity of annealed and unannealed gold films, Optics Express 2016;24:19254–63.
[68] Carpene E. Ultrafast laser irradiation of metals: beyond the two-temperature model. Phys Rev B 2006;74:024301.
[69] Ashcroft N, Mermin N. Solid state physics. Fort Worth, Saunders College Publishing, 1976.
[70] Pells G, Shiga M. The optical properties of copper and gold as a function of temperature. J Phys C 1969;2:1835.
[71] Chen Y-J, Lee M-C, Wang C-M. Dielectric function dependence on temperature for Au and Ag. Jpn J Appl Phys 2014;53:08MG02.
[72] Reddy H, Guler U, Kildishev A, Boltasseva A, Shalaev V. Temperature-dependent optical properties of gold thin films, Optical Materials Express, 2016;6:2776–802.
[73] Sundari S, Chandra S, Tyagi A. Temperature dependent optical properties of silver from spectroscopic ellipsometry and density functional theory calculations. J Appl Phys 2013;114:033515.
[74] Bohren C, Huffman D. Absorption and scattering of light by small particles. New York, Wiley & Sons, 1983.
[75] Yeshchenko O, Bondarchuk I, Gurin V, Dmitruk I, Kotko A. Temperature dependence of the surface plasmon resonance in gold nanoparticles. Surf Sci 2013;608:275–81.
[76] Amendola V, Meneghetti M. Laser ablation synthesis in solution and size manipulation of noble metal nanoparticles. Phys Chem Chem Phys 2009;11:3805–21.

[77] Bhattacharya A, Mahajan R. Temperature dependence of thermal conductivity of biological tissues. Physiol Meas 2003;24:769–83.
[78] Pollack G. Kapitza resistance. Rev Mod Phys 1969;41:48–81.
[79] Duda J, Yang C-Y, Foley B, Cheaito R, Medlin D, Jones R, Hopkins P. Influence of interfacial properties on thermal transport at gold:silicon contacts. Appl Phys Lett 2013;102:081902.
[80] Polavarapu L, Venkatram N, Ji W, Xu Q-H. Optical-limiting properties of oleylamine-capped gold nanoparticles for both femtosecond and nanosecond laser pulses. ACS Appl Mater 2009;1:2298–303.
[81] Lalisse A, Tessier G, Plain J, Baffou G. Quantifying the efficiency of plasmonic materials for near-field enhancement and photothermal conversion. J Phys Chem C 2015;119:25518–28.